Naval Research Laboratory

Washington, DC 20375-5320

NRL/MR/6111--97-8116

Particle Size and Surface Area Analysis of Amorphous and Crystalline Boron

JANE K. RICE

Chemical Dynamics and Diagnostics Branch
Chemistry Division

December 10, 1997

REPORT DOCUMENTATION PAGE

Form Approved
OMB No. 0704-0188

1. AGENCY USE ONLY (*Leave Blank*)	2. REPORT DATE	3. REPORT TYPE AND DATES COVERED
	December 10, 1997	Interim Report

4. TITLE AND SUBTITLE

Particle Size and Surface Area Analysis of Amorphous and Crystalline Boron

5. FUNDING NUMBERS

6. AUTHOR(S)

Jane K. Rice

7. PERFORMING ORGANIZATION NAME(S) AND ADDRESS(ES)

Naval Research Laboratory
Washington, DC 20375-5320

8. PERFORMING ORGANIZATION REPORT NUMBER

NRL/MR/6111--97-8116

9. SPONSORING/MONITORING AGENCY NAME(S) AND ADDRESS(ES)

ARI in Energetic Materials, Naval Research Laboratory
Office of Naval Research
800 North Quincy Street, Arlington, VA 22217-5660

10. SPONSORING/MONITORING AGENCY REPORT NUMBER

11. SUPPLEMENTARY NOTES

12a. DISTRIBUTION/AVAILABILITY STATEMENT

Approved for public release; distribution unlimited.

12b. DISTRIBUTION CODE

13. ABSTRACT (*Maximum 200 words*)

Surface areas were measured and scanning electron microscopy (SEM) photographs were obtained from seven boron particle samples used in recent boron particle combustion experiments. Some significant differences were seen between the manufacturer claimed particle sizes and the distributions obtained from the SEM photographs. In those samples with large particle size distributions, calculated surface areas differed significantly from measured surface areas and it is clear that a single particle diameter parameter is inadequate to describe the corresponding surface area of the true particle size distribution. In general, the particle size distribution estimates taken from SEM yield lower surface areas than were measured. Further data on the purity of the samples are necessary to determine whether the phase or purity of the boron particle has an effect on the efficiency of boron particle combustion.

14. SUBJECT TERMS

Boron
Particle combustion
Scanning electron microscopy
Surface area

15. NUMBER OF PAGES

33

16. PRICE CODE

17. SECURITY CLASSIFICATION OF REPORT	18. SECURITY CLASSIFICATION OF THIS PAGE	19. SECURITY CLASSIFICATION OF ABSTRACT	20. LIMITATION OF ABSTRACT
UNCLASSIFIED	UNCLASSIFIED	UNCLASSIFIED	UL

NSN 7540-01-280-5500

Standard Form 298 (Rev. 2-89)
Prescribed by ANSI Std 239-18
298-102

CONTENTS

PARTICLE SIZE AND SURFACE AREA ANALYSIS OF AMORPHOUS AND CRYSTALLINE BORON

ABSTRACT

Surface areas were measured and scanning electron microscopy (SEM) photographs were obtained from seven boron particle samples used in recent boron particle combustion experiments. Some significant differences were seen between the manufacturer's claimed particle sizes and the distributions obtained from the SEM photographs. In those samples with large particle size distributions, calculated surface areas differed significantly from measured surface areas and it is clear that a single particle diameter parameter is inadequate to describe the corresponding surface area of the true particle size distribution. In general, the particle size distribution estimates taken from SEM yield lower surface areas than were measured. Further data on the purity of the samples are necessary to determine whether the phase or purity of the boron particle has an affect on the efficiency of boron particle combustion.

INTRODUCTION

Solid boron is a dense, energetic material with a large heat of fusion and has been under scrutiny for over 30 years as a potential solid or liquid propellant additive. The potential energy release from boron-containing fuels is about 36% greater in cal/g than the liquid hydrocarbon fuel JP5 and 86% greater than solid fuels containing metallic aluminum. When calculated on a volumetric basis in units of cal/cm^3, boron is 3.9 times more energetic than JP5.[1]

Boron combustion occurs in two stages. Due to the high melting point of solid boron (2400 K) and the equally high vaporization point of B_2O_3, the first stage of boron combustion is inhibited by a thin film of liquid B_2O_3 that forms on the outer surface of the boron particle. This film remains until temperatures greater than 2400 K are reached, the film vaporizes, and combustion proceeds more rapidly. The second stage of boron combustion begins when the pure boron material freely combusts at the higher temperatures. Several groups have measured ignition of boron particles under various conditions. Macek et al.[2,3] carried out work in a flat flame burner at medium pressures using laser ignition. Li and Williams [4,5] examined small particles in a flat flame burner at low pressure. Yuasa and Isoda[6] obtained spatially resolved spectra of flash-ignited boron particles in a stagnation stream. Expansion into the high pressure regime has been carried out by Krier, Foelsche, and coworkers. Krier et al.[7] examined the effect of pressure on ignition and combustion in a shock tube apparatus. Foelsche et al.[8] examined the combustion of boron in hydrogen/oxygen/water vapor mixtures at 1360 atm and 3800 K in a combustion bomb.

There is some controversy over the details of the first and second stage and how the $B_2O_3(\ell)$ layer is formed. Based on theoretical calculations, Glassman[9] concluded that in stage 1, the boron oxide is formed by the dissolution of pure boron outward through the $B_2O_3(\ell)$ layer. However, King[10-12] modeled the problem by assuming O_2 diffuses inward through the $B_2O_3(\ell)$ to reach the B/ B_2O_3 interface. Recent measurements and

Manuscript approved October 21, 1997

modeling by Yeh and Kuo[13] support the former description. Using environmental scanning electron microscopy (ESEM), nonconductive surfaces were detected. With this they observed the melting of boron particles at a temperature of 950 K, far lower than the melting point of boron and higher than the melting point of B_2O_3. They observed a polymeric vitreous $(BO)_n$ complex formed by the reaction of dissolved boron and molten $B_2O_3(\ell)$, and report the dependency of first-stage combustion times on ambient gas temperature, ambient species concentration, and chamber pressure. The pressures included in the modeling were in the range of 1 to 35 atm. Foelsche et al.[8] support a model in which the diffusion of O_2 into the boron/$B_2O_3(\ell)$ layer occurs during the first stage. This is based on the fact that they saw a two times increase in ignition delay with a reduction of 5% in the O_2 mole fraction. Their data were collected under conditions of high temperature (1400 to 3400 K) and pressure (peak of 157 atm).

During combustion, a variety of gas-phase products are produced including but not limited to BO, BO_2, B_2O_2, BOH, and HOBO.[14-16] The lowest energy, and therefore, the most desired product is B_2O_3. The reaction from solid boron to liquid B_2O_3 is exothermic by 300 Kcal/mol and is shown in Eq. (1).

$$2\,B(s) + 3/2\,O_2 \rightarrow B_2O_3(\ell) \qquad (1)$$

This is the most efficient pathway in the combustion of boron. The more realistic and undesired scenario is to form a variety of species other than B_2O_3, for example, HOBO. The gas-phase modeling of boron combustion is based on chemical kinetics code packages developed at Sandia called CHEMKIN[17] and SENKEN.[18] Fluorine chemistry has been added recently by Yetter et al.[14] and Brown et al.[15] to demonstrate that enhancement of complete combustion can occur when HF and other fluorinated compounds are added to the pool of reactants. A few other approaches have been investigated to try to enhance the performance of boron combustion. One of these is to add a thin layer of titanium or other metal to the surface of the boron particle to heat the surface faster, and hence, reach the second stage of combustion faster.[19,20]

It has been suggested that one difference in boron particle combustion performance may be the phase and related purity of the boron material. In general, it has been difficult to generate amorphous material with as high a purity as crystalline material. Whether there is a phase/purity related difference in performance remains controversial because few controlled experiments have been done to prove or disprove this hypothesis. Much of the older literature and some of the newer literature are complicated by the fact that boron samples are not fully characterized and in cases where characterization is done, the results are conflicting. Small impurities appear to strongly affect some of the physical properties of boron.[21] Literature in the 1960's and 1970's is difficult to interpret but folklore suggests that contaminants in amorphous samples were the cause of increased performance. These difficult questions of physical properties and purity cloud the literature and remain unanswered today.

In this report, seven samples of amorphous and crystalline boron that recently have been used in various combustion and detonation experiments are analyzed by SEM and surface area analysis. The boron particles were examined by SEM to determine the general physical features and the particle size distribution. An estimated surface area (m^2/ gm) was calculated from the measured particle size distribution. The actual surface area was then experimentally measured using a Monosorb instrument (Quantachrome Corp.) and analyzed using a single-point BET (Brunauer, Emmett and Teller) analysis.[22] The actual and calculated surface areas are compared and discussed in terms of recent particle combustion results.

Yeh and Kuo[13] have theorized that if the particle reactions are diffusion controlled, the particle diameter has a larger effect ($\propto d^2$) on the combustion time. However, if kinetically controlled, the combustion time is linear with particle diameter ($\propto d$). The two pathways are equal when the Damköhler number equals one or $P*d_p/75$ equals one, where P is in atm and d_p is in μm. Therefore, the lower the pressure, the more influence the surface area will have. One way to increase the surface area is to decrease the particle size.

EXPERIMENT

Boron Samples

Table 1 lists the seven samples that were analyzed in this study. These samples provided a variety of surface areas from stocks that had been used in boron combustion experiments.

Surface Area Measurements

The surface area measurements were made using a Monosorb instrument that uses a single-point BET algorithm.[22] A mixture of 30% nitrogen (by volume) with the balance helium is used as the adsorbate. A sample of about 0.25 to 0.3 grams was degassed at 18°C for 45 min prior to measuring the surface area to remove water and adsorbed gases at the surface. The sample was then cooled to liquid nitrogen temperatures and the adsorbate adhered to the boron surface. Once at equilibrium, the sample was heated and the adsorbate was quickly desorbed. The flow of gas out of the sample was measured with thermal conductivity detectors and the surface area was calculated from the amount and cross sectional area of the adsorbate released. The measurement was carried out at a partial pressure of adsorbate of about 0.3. This ensured that a monolayer had formed on the surface and allowed the calculation of the surface area based on the cross-sectional area of the adsorbate. The amount of gas released was converted to units of square meters. The sample was then weighed and the surface area reported in units of square meters per gram. The accuracy of the single-point BET measurement is generally on the order of 5%. The reproducibility is ~1 to 2%.

RESULTS

Scanning Electron Microscopy

Scanning electron microscopy was carried out on a Hitachi, Model S400 at 15 to 20 kV at magnifications from 400x to 30,000x. Sample 1 was coated with spuddered gold-palladium for improved contrast and is shown in Fig. 1. The particles are spherical in appearance and relatively uniform with d_p's ~ 0.08 to 0.1 μm. Sample 2 is shown in Fig. 2. It appears to be identical in size and structure to sample 1. Figures. 3(a) and 3(b) are that of sample 3, indicating a larger size distribution than samples 1 and 2. Figures 4(a) and (b) represent the crystalline boron sample 4, which is 0.08 to 8.0 μm in particle size and appears as a very wide distribution of irregularly shaped crystals. Figures 5(a) and (b) represent a crystalline boron sample similar to sample 4. Figures 6(a) and 6(b) represent crystalline boron with d_p's from 0.08 to 35.0 μm. Figures 7(a) and 7(b) represent a sieved sample of larger crystalline boron particles with d_p's between 20 and 25 μm. However, as can be seen in Fig. 7(b), there are numerous small particles which adhere to the larger crystalline surfaces which are not removed by sieving.

Table 1
Particle Sizes and Surface Areas of Amorphous and Crystalline Boron

Sample Number	Sample Source	Sample Type and Purity(%)	Nominal Size, d_p (μm)[a]	Measured Surface Area (m^2/g)[b]	Calculated Surface Area Corresponding to $d_{Sauter(32)}$ or $d_{single-value}$ (m^2/g)[c]	Ratio of Measured to Calculated Surface Area[d]
1	P. Zavitsanos/ Callery	Amorphous, 99.5	d_p<1	38 ± 3	30 (single valued)	1.3
2	H. Krier/Alfa AESar	Amorphous, unknown	d_p<0.1	35 ± 5	30 (single valued)	1.2
3	K. Kuo & C.Yeh/Atlantic	Amorphous, 93	d_p~2-3	12 ± 2	3.2 (distribution)	3.7
4	T. Russell/ Thiokol	Crystalline, 99.5	d_p<1.0	4.2 ± 0.2	0.88 (distribution)	4.8
5	K. Kuo & C.Yeh/Noah	Crystalline, 99.5	d_p~3	1.6 ± 0.3	0.67 (distribution)	2.4
6	H. Krier/ Goodfellow	Crystalline, 99.6	d_p< 20	0.95 ± 0.2	0.28 (distribution)	3.4
7	H. Krier/ Aldrich	Crystalline, 99.0	20<d_p<25 sieved	0.12 ± 0.02	0.10 (single valued, d_p=25)	1.2
					0.079 (distribution)	1.5

a) Size given by the manufacturer.

b) Two to four measurements taken and averaged and given with statistical error. Systematic error expected to be less than 5%. The diameters corresponding to the measured surfaces areas are 0.21, 0.61, 2.7, 2.7, and 21 for samples 3 through 7, respectively.

c) This calculation assumes a smooth, perfect sphere and represents a minimum calculated value for the surface area.

d) Ratios of m^2/g were used.

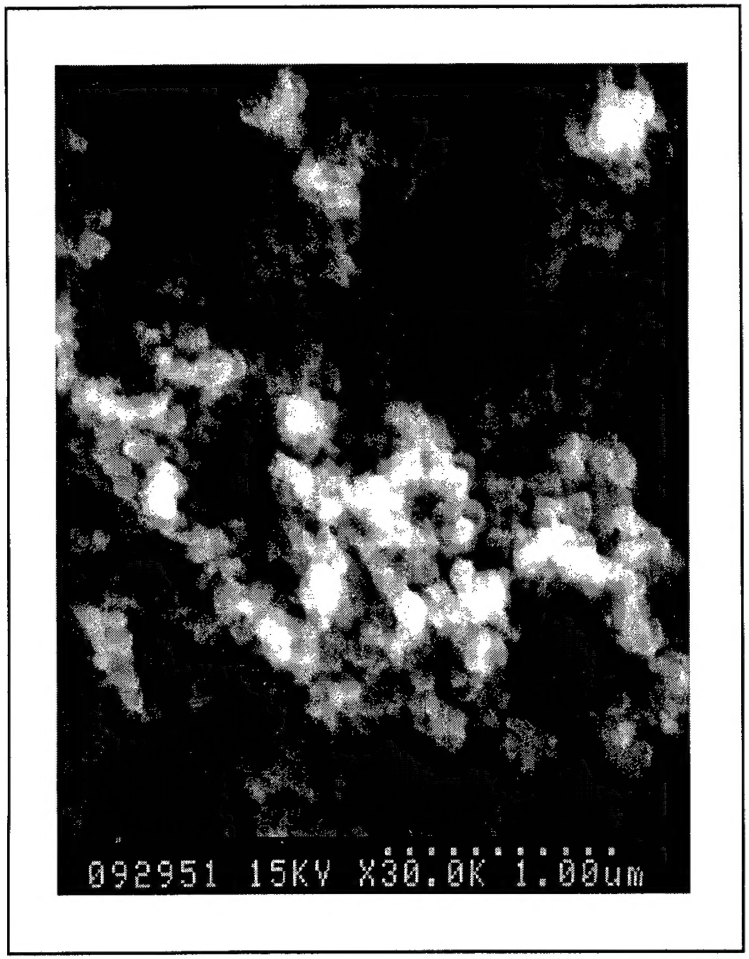

Fig. 1-Shown is a SEM photograph of sample 1, amorphous boron, from Zavitsanos. It is coated with spuddered gold-palladium for improved contrast. It was taken at 15 kV with a magnification of 30,000x. A 1 μm scale is given by dots in the lower right hand corner.

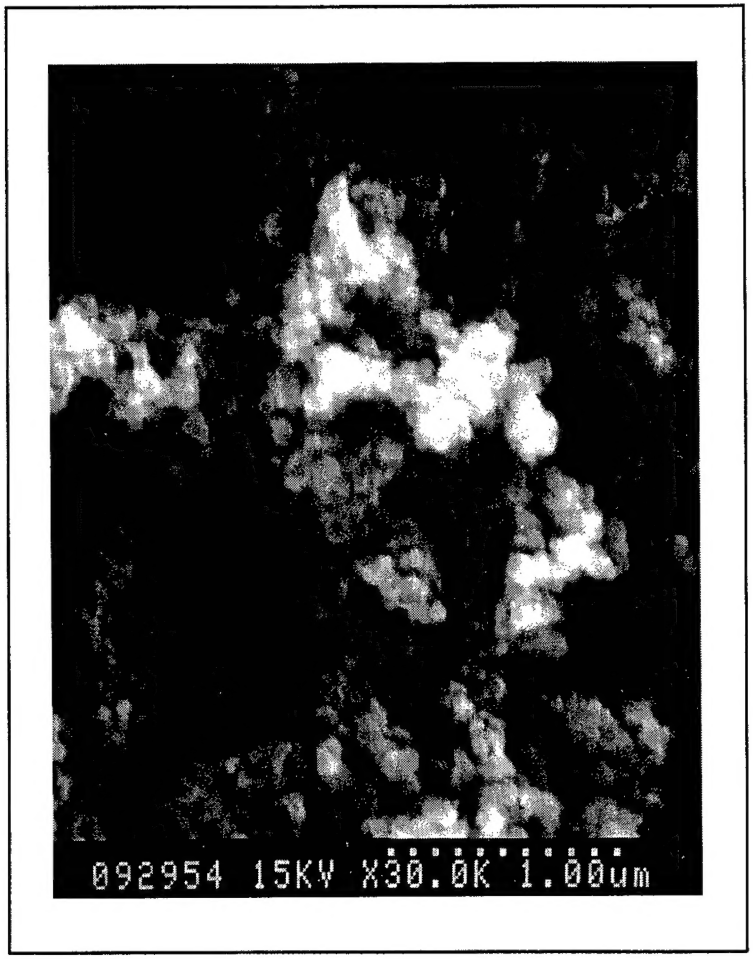

Fig. 2- Shown is a SEM photograph of sample 2, amorphous boron from Krier, with a magnification of 30,000x.

Fig. 3(a) Shown is a SEM photograph of sample 3, amorphous boron from Kuo and Yeh, with a magnification of 4,000x.

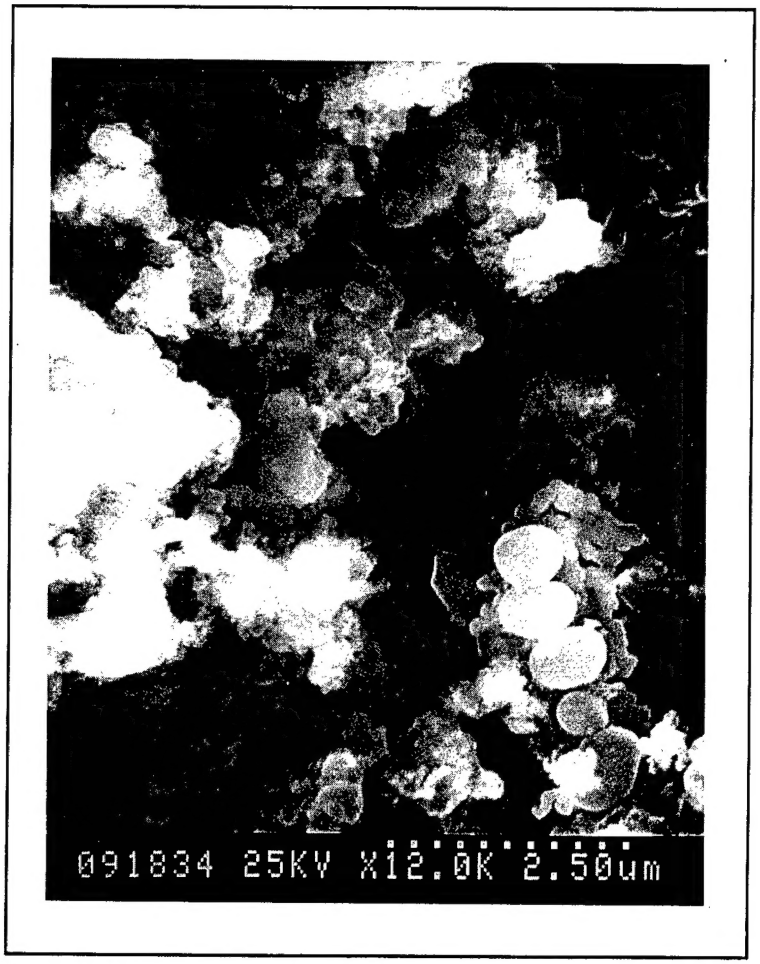

Fig. 3(b)-Shown is a SEM photograph of sample 3, amorphous boron from Kuo and Yeh, with a magnification of 12,000x.

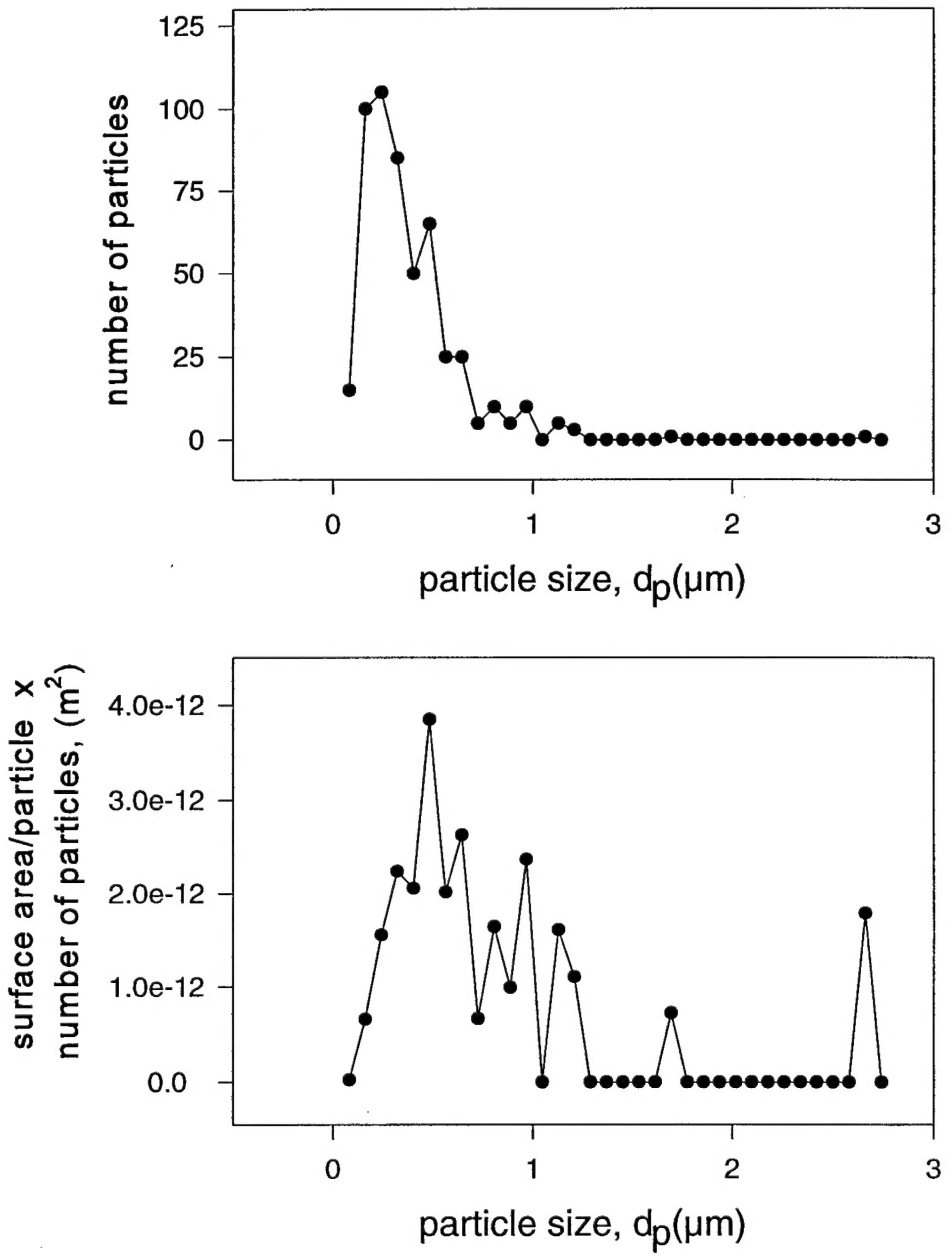

Fig. 3(c)-The upper plot shows the particle size distribution of sample 3 and the lower plot shows the surface area of the total particle size distribution normalized by the interval size. See Appendix A for a tabular list.

Fig. 4(a)-Shown is a SEM photograph of sample 4, crystalline boron from Russell, with a magnification of 3,000x.

Fig. 4(b)-Shown is a SEM photograph of sample 4, crystalline boron from Russell, with a magnification of 15,000x.

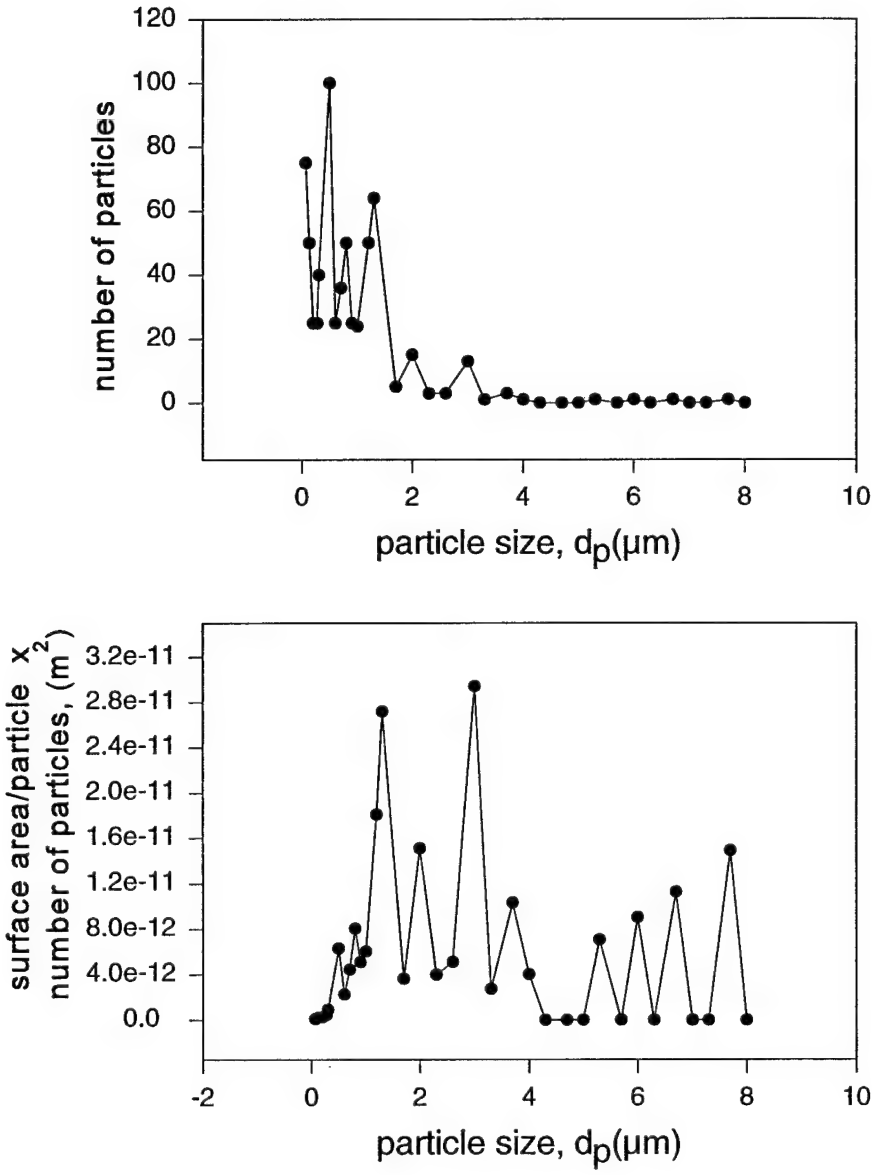

Fig. 4(c)-The upper plot shows the particle size distribution of sample 4 and the lower plot shows the surface area of the total particle size distribution normalized by the interval size.

Fig. 5(a)-Shown is a SEM photograph of sample 5, crystalline boron from Kuo and Yeh, with a magnification of 2,000x.

Fig. 5(b)-Shown is a SEM photograph of sample 5, crystalline boron from Kuo and Yeh, with a magnification of 6,000x.

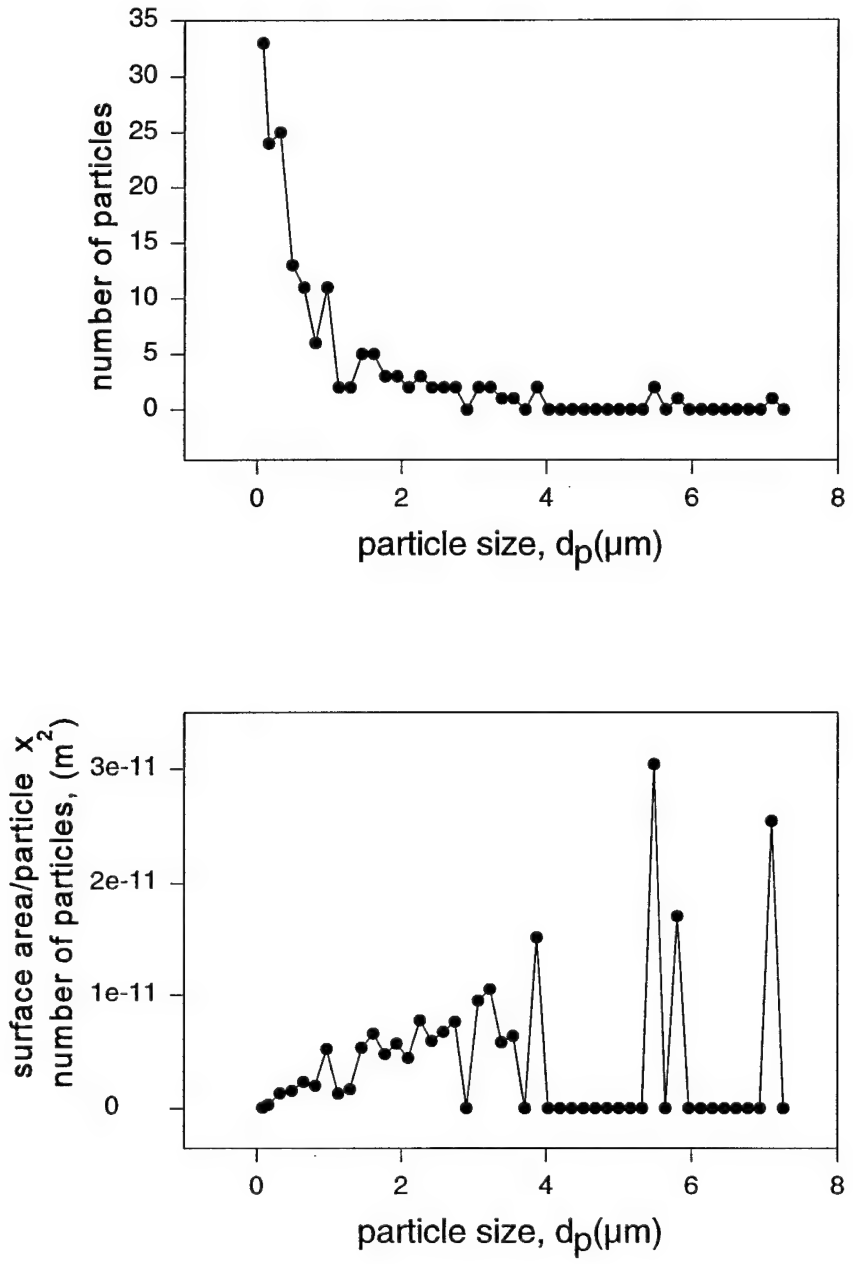

Fig. 5(c)-The upper plot shows the particle size distribution of Sample 5 and the lower plot shows the surface area of the total particle size distribution normalized by the interval size.

Fig. 6(a)-Shown is a SEM photograph of sample 6, unsieved crystalline boron from Krier, with a magnification of 400x.

Fig. 6(b)- Shown is a SEM photograph of sample 6, unsieved crystalline boron from Krier, with a magnification of 6,000x.

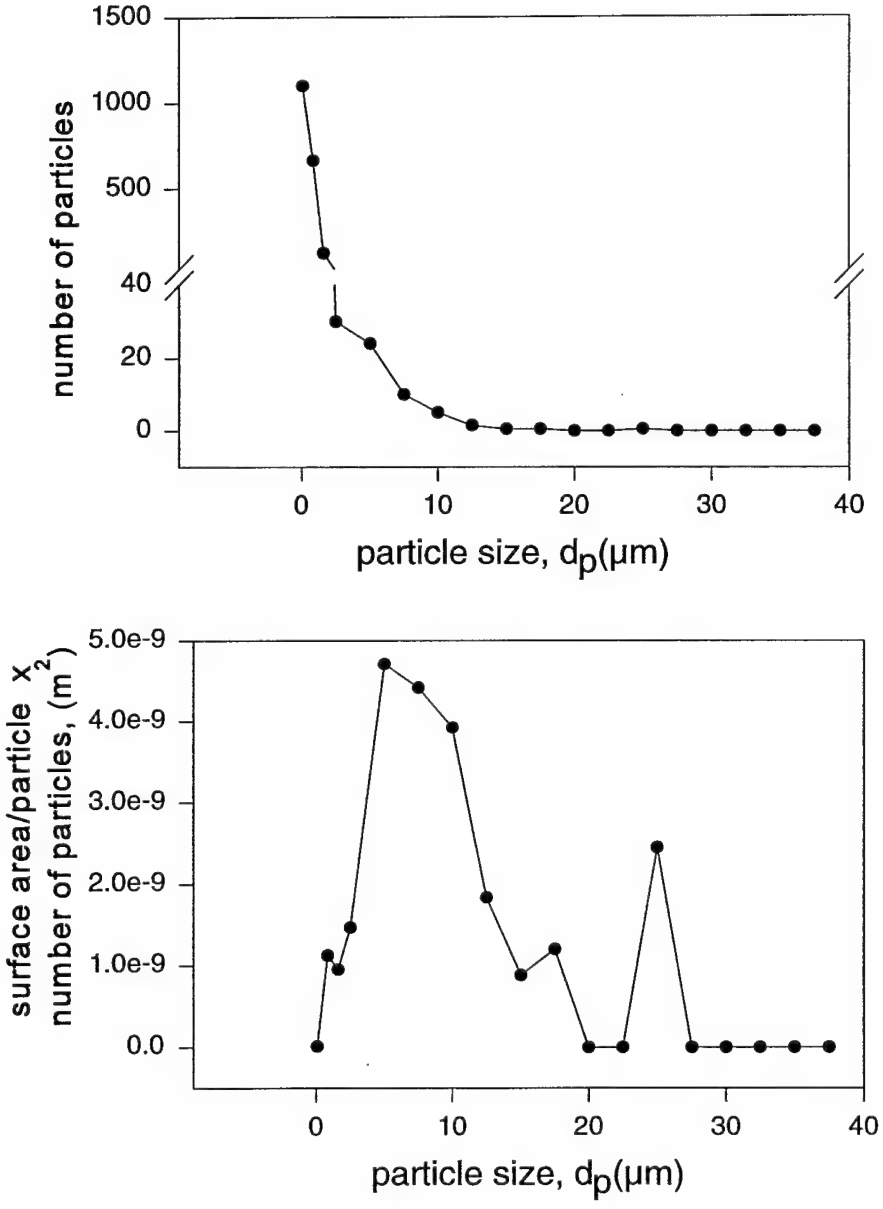

Fig. 6(c)-The upper plot shows the particle size distribution of sample 6 and the lower plot shows the surface area of the total particle size distribution normalized by the interval size.

Fig. 7(a)-Shown is a SEM photograph of sample 7, sieved crystalline boron from Krier, with a magnification of 400x.

Fig. 7(b)-Shown is a SEM photograph of sample 7, sieved crystalline boron from Krier, with a magnification of 6,000x.

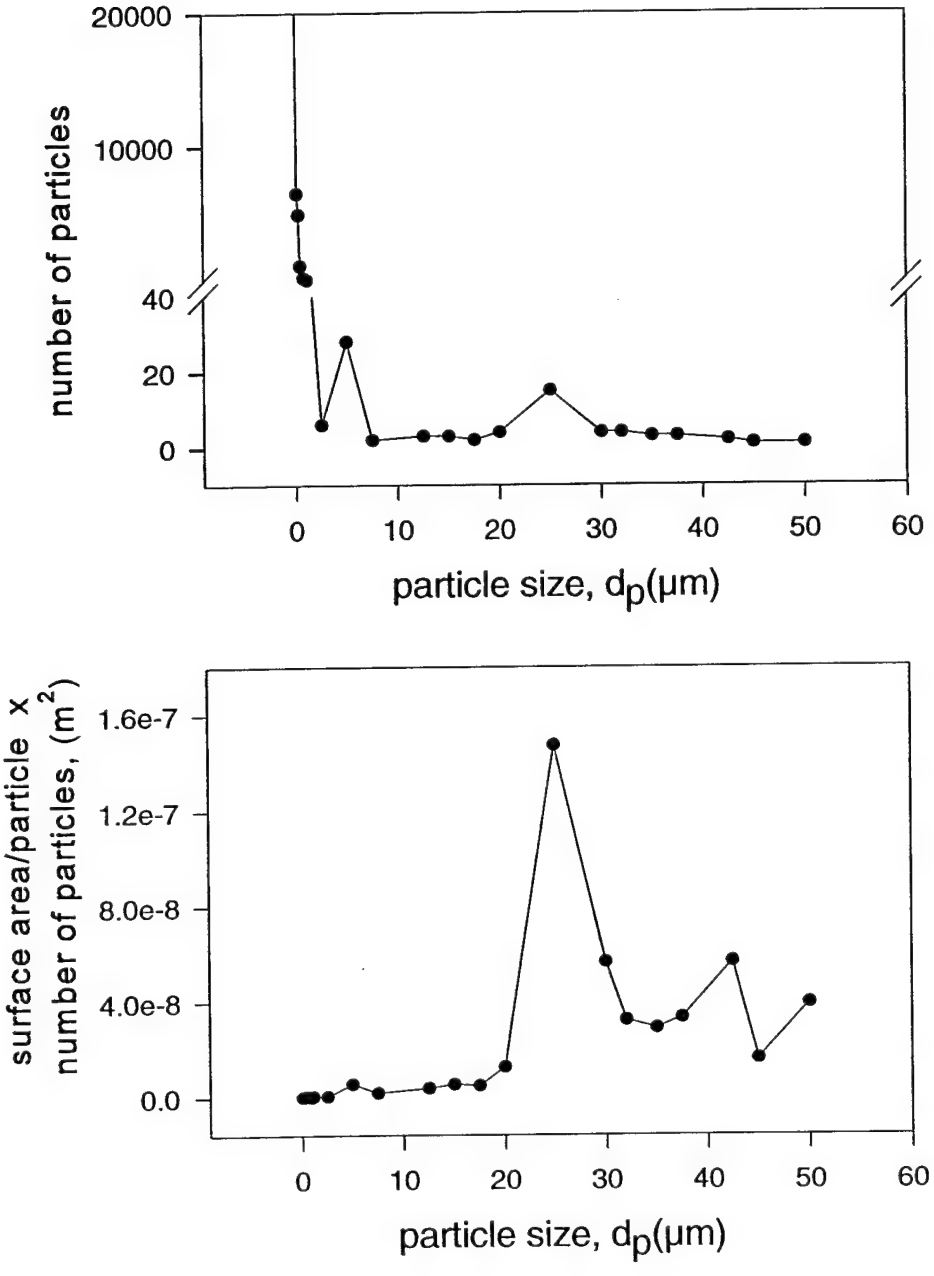

Fig. 7(c)-The upper plot shows the particle size distribution of sample 7 and the lower plot shows the surface area of the total particle size distribution normalized by the interval size.

Estimating the Size Distribution of Particles

Samples 1 and 2 contained amorphous particles that were uniform and spherical, therefore, the size distribution was represented by a Delta function. The particle size of highest occurrence, $d_p(max)$, was 0.85 μm. In sample 3, the particles were not uniform and a distribution determined from SEM was required to describe the particle sizes. For each of the crystalline boron samples 4 through 6, the distribution of particles was broad and also required an estimate of the distribution from SEM photographs. Both the Delta function and distribution methods were applied to sample 7. Table 2 lists the observed particle size distributions; the 10%/90% particle size distribution; the most probable particle size, $d_p(max)$; the d_{20} particle diameter in which the surface area is normalized to the number of particles; and the d_{32} particle diameter, also known as the Sauter diameter, in which the total surface area is normalized to the mass of the particle ensemble. Reference 23 and Appendix A discuss these diameters.

Particle size distributions were obtained by manually counting the particles in the SEM photographs. A minimum of 100 particles was counted in each sample to obtain the distributions. In sample 3, larger sized particles were counted from an area of 288 μm^2, where 7.5 μm equaled 3.1 cm in the photograph. Smaller particles were counted in an area of 30.2 μm^2 where 2.5 μm equaled 3.1 cm. The counts in these areas were then multiplied by the ratios of the areas to arrive at the total particle distribution in the 1022 μm^2 area. The particle diameters were measured in one dimension along one axis of the photograph. Since the particles were of random shapes, and were randomly positioned in the photo, this simpler measurement was assumed to give an average particle diameter. The particles were then assumed to be spherical, which represents a minimum calculated surface area for the particles observed since any deviation away from a perfect sphere will lead to a larger surface area.

In sample 4, large particles were counted in a photographed area of 29.2 by 35 μm equaling 1022 μm^2, where 10 μm corresponds 30 mm in the photograph. Mid-sized particles were counted in an area of 511 μm^2 and small particles were counted in an area of 41 μm^2. Figure 4(c) is a plot of the particle distribution for this sample. In sample 5, large particles were counted in an area corresponding to 246 μm^2 (1/9th the area of that of Fig. 5(a)) and small particles were counted from all of Fig. 5(b), also corresponding to 246 μm^2. The particle size distribution of sample 6 was counted similarly. An area of 10,900 μm^2 was used to count the larger particles and an area of 254 μm^2 was used for the smaller particles. The total distribution of particles for 5450 μm^2 is shown in Fig. 6(c). The particle size distribution of sample 7, sieved crystalline boron, is shown in Fig 7(c). The distribution of particles were obtained from the SEM photographs 7a and b in a similar manner described for Sample 6, however, an area of 5450 μm^2, not 10,900 μm^2, was used. Seventy-five microns corresponds to 30 mm in Fig. 7(a) and 5 μm corresponds to 30 mm in Fig. 7(b).

Estimating the Surface Area from the Size Distributions of the Particles

Using the particle size distributions obtained from SEM photos, and assuming the particles have a spherical shape, the surface area of each boron sample in units of m^2/g was calculated. Larger particles have larger surface areas, however, smaller particles have larger surface areas per gram. A plot of the surface area per particle as a function of particle diameter is shown in the upper plot of Fig. 8. This surface area was multiplied by the number of particles to obtain the total surface area shown in the lower plots of Figs. 3(c), 4(c), 5(c), 6(c), and 7(c). This was related to the number of grams in the sample by calculating the number of grams of boron material present in the photographs from the particle diameter, particle distribution, and the density of boron (2.34 g/cm^3). To calculate the surface area of uniformly sized particles, the following

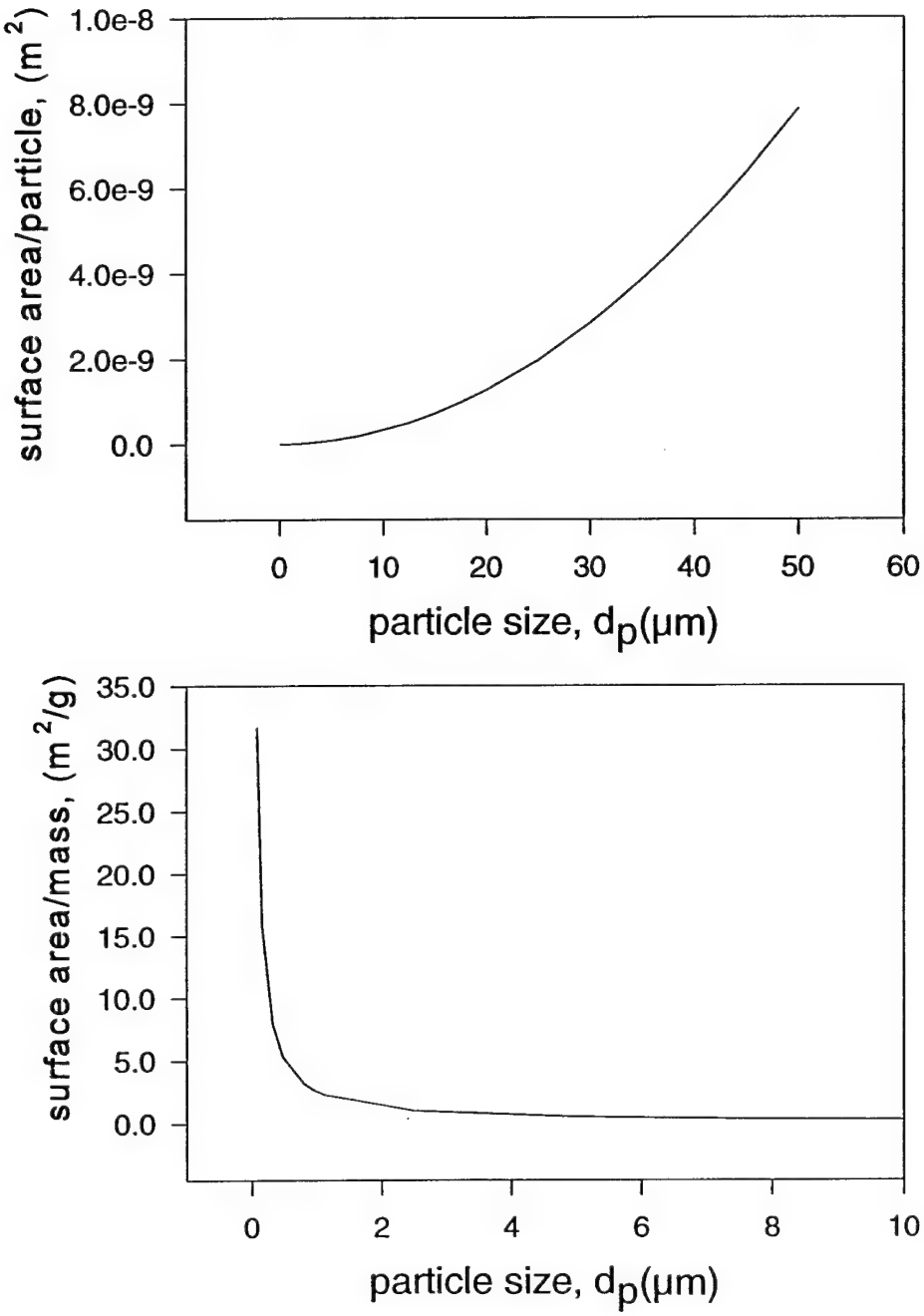

Fig. 8-The upper plot shows the surface area of a simple spherical particle as a function of particle size and the lower plot shows the surface area per gram of a simple sphere as a function of particle size.

equation derived from the surface area, volume of a sphere, and density was used

$$2.56/d_p(\mu m) = \text{surface area } (m^2/g). \quad (2)$$

A general plot of surface area per gram of boron as a function of particle diameter is shown in the lower plot of Fig. 8. The specific particle sizes, numbers of particles, surface areas, and related calculations for the seven samples are given in Appendix A.

Errors in the estimate of the surface area of the boron samples are due to several assumptions. The photographs are assumed to be representative of the sample at large and all particle sizes are assumed to be equally visible in the photographs. The latter is probably not the case since larger particles were probably preferentially counted because they obscure smaller particles. I also assumed the particles to be perfect spheres, which led to a lower estimated surface area than the actual surface area. This assumption is a poor one if the sample contains grossly irregular particles. For example, if the shape is cubic instead of spherical, the ratio of the true surface area to the calculated surface area will be 1.24. This assumes the volumes of the square and sphere are the same. The ratio can be as high as 2.3 if the diameter of the sphere is assumed to be the side length of the cube.

Comparison of Estimated and Measured Surface Areas

Table 1 contains the measured and estimated surface areas for the samples in this study. The boron samples are listed in order of decreasing BET measured surface area in column 5. Two different diameters are listed in Table 2. The surface diameter, d_{20}, corresponds to the total surface area divided by the total particle number. The Sauter diameter, d_{32}, corresponds to the ratio of the sum of the surface area to the sum of the mass of the particles.[23] Therefore, one is normalized by the particle number and the other by the particle mass or volume. Appendix A presents the details of how the diameters are obtained.

The calculated surface area is expected to be somewhat lower than the measured surface area due to the spherical particle assumption discussed previously. In the case of the first two amorphous samples, which resemble spheres, the differences are expected to be low. The calculated values are only 1.3 and 1.2 times that measured for samples 1 and 2, respectively. Sample 3 has a higher value of 3.7 and this is partially attributed to some nonspherical characteristics in the SEM but primarily due to a larger distribution of particle sizes and errors associated with counting the particles. The SEM reveals what appears to be clustering, making it more difficult to count the particles or determine their actual size. The crystalline samples exhibit wide distributions of particle size and vary considerably from spherical. A correction from spherical to cubical would yield calculated surfaces about 1.7 times higher. In the case of sample 6, however, it would appear that the difference is due to a miscounted distribution since the sieved sample, which is more homogeneous, is very close to the measured surface area. On the other hand, the act of sieving may select rounder particles and so we are not able to clearly attribute the underestimation of the calculated surface areas to one particular cause.

Sample 4 has the worst match between measured and calculated surface area. It may have a more rugged surface, however a slight miscounting of very large particles can strongly affect the calculated surface area. Samples 4 and 5 have similar distributions in Table 2 and in Figs. 4 and 5, however the measured BET

surface areas differ significantly, 4.2 and 1.6 m^2/g, respectively. This demonstrates the importance of the surface area measurement.

Sample 7's distribution was calculated first by assuming a single value for the size of the particles and, second, by counting the distribution of the particles. Both are relatively accurate. The distribution is slightly underestimated. The third contribution to the errors in these calculations may be a bias from not fully counting smaller sized particles. This error would be larger for larger distributions of particle size.

CONCLUSIONS

Several conclusions can be drawn from comparisons between calculated and measured surface area. When there is a wide spread of particle sizes, even a counting method based on SEM photos can have moderate errors. An estimate of the surface area from the radius of the particle yields a minimum surface area that can be 4 to 5 times lower than obtained from the BET measurement. The BET measured surface area provides an indisputable comparison of the surface area available for each of the samples and it accentuates the difficulty in getting accurate particle size distributions. This experiment also demonstrates the difficulty in obtaining well-characterized, narrowly distributed particles for combustion experiments. For example, even after careful sieving, smaller particles are shown to adhere to the surface of samples 6 and 7, as previously reported by Foelsche et al.[8]

All the crystalline samples examined here have larger particle sizes and lower surface areas than the amorphous samples. The minimum difference is a factor of 3 between samples 3 and 4. If combustion experiments determine that amorphous boron leads to more efficient combustion, these studies must be followed by experiments comparing amorphous and crystalline material in which differences in particle surface areas are eliminated. If combustion experiments determine that crystalline boron leads to more efficient combustion, going to smaller crystalline particles to increase the surface area may still improve performance. However, if surface area and not phase or purity is the most important performance factor, the amorphous material studied here should perform better based on its significantly higher surface area.

Amorphous boron is generally less pure than crystalline boron. However, sample 1 is reported to be 99.5% pure, which is as pure as the crystalline samples are reported to be. It may be useful to have elemental analysis done on the samples to verify the reported purities, however, I did not have enough material for these tests. The impurities in sample 3 are reported to be primarily magnesium.[13] As described by Neslain,[24] the particular impurities depend on the synthesis process used. In general, these impurities include C, O, Mg, Al, Si, Ca, and Fe.[21] Goodfellow reports impurities of Fe, C, O, N, and H in their 99.6% pure crystalline powder of < 150 μm diameter.

Using the model of Yeh and Kuo,[13] the combustion time in the first stage should increase proportionally to the particle diameter. In the second stage the combustion time should increase either proportionally (kinetically controlled - small particles at low pressure) or increase as the square of the particle diameter (diffusion controlled - larger particles at high pressure). For accurate fitting of the rate data, the surface areas must be determined accurately. This report demonstrates that a direct surface area measurement provides an accurate way of comparing different boron samples.

Table 2
Boron Particle Distributions of Amorphous and Crystalline Boron

Sample Number	Observed Particle Size Distribution, from SEM, d_p (μm)[a]	10/90 Particle Distribution (μm)	Particle Size at Population Distribution Maxima, d_p(max) (μm)	$d_{Surface(20)}$ from Particle Distributions	$d_{Sauter(32)}$ from Particle Distributions	Calculated Surface Area Corresponding to $d_{Sauter(32)}$ or $d_{single\text{-}value}$ (m^2/g)
1	0.08- 0.1	assumed single-valued	0.085 single-valued	-	-	30
2	0.08- 0.1	assumed single-valued	0.085 single-valued	-	-	30
3	0.08-2.7	0.2/0.6	0.24	0.45	0.80	3.2
4	0.08- 8.0	0.2/2.3	0.50	1.1	2.9	0.88
5	0.08-7.3	0.08/2.4	≤ 0.08	1.6	3.8	0.67
6	0.08- 38	0.08/1.6	≤ 0.08	2.3	9.1	0.28
7	0.08- 50	0.08/0.3	0.3 (first) 25 (second)	-	-	0.10[b]
				5.6	32	0.079

a) The 0.08 μm diameter is near the lower limit of detection.
b) Based on a single-valued diameter of 25 μm.

Foelsche et al.[8] report no difference in ignition times between 1 μm and 24 μm crystalline boron particles under high temperature (2450 K) and high pressure (8 to 65 atm) conditions. Samples 4 and 7, respectively, were used in their study. The surface areas of these samples differ by a factor of 35. Others have also reported an insensitivity to particle size.[3,5,7]

Rice and Russell[25] have observed more complete combustion products from crystalline boron (sample 4) than amorphous boron (sample 1) under high-pressure (30 Kbar), laser-initiated experiments. The reactions of boron with PETN and PETN-NF_2 were compared. Several factors may play a role in these experiments. First, it is difficult if not impossible to quantify the amount of boron. Second, phase changes may occur at the higher pressures. The crystalline sample clearly underwent more complete combustion under high-pressure, low-temperature quenching conditions, although the crystalline sample had 1/9th the surface area of the amorphous sample. These factors must be kept constant or controlled to draw further conclusions from this anecdotal study.

Data and modeling from Yeh and Kuo[13] taken with data from Macek[3] indicate a decrease in combustion burn time with smaller particle size under low pressure conditions. It may be that higher pressures are the overriding factor in the combustion times of the Foelsche et al.[8] and the Rice and Russell[25] experiments. In any case, better information regarding the actual surface areas of the samples reported here will hopefully clarify some of the remaining boron particle combustion issues surrounding purity and the effect of particle size.

ACKNOWLEDGMENTS

I would like to thank Dr. Jim Horwitz for obtaining several of the SEM scans. I thank Drs. Tom Russell, Herman Krier, Peter Zavitsanos, Ken Kuo and Jerry Yeh for suppling the boron samples. I thank Dr. Jacques Boileau for providing boron references related to boron purity. I would like to acknowledge the ARI in Energetic Materials at NRL and ONR for support of this work. I thank those who attended the Boron Chemistry Pennsylvania State Workshop in 1996 for interesting discussions on the issue of boron sample purity.

REFERENCES

1. G.M. Faeth, "Status of Boron Combustion Research," Air Force Office of Scientific Research Report (1984).

2. A. Macek and J.M. Semple, "Combustion of Boron Particles at Atmospheric Pressure," *Combustion Science and Technology* **1**, pp. 181-191 (1969).

3. A. Macek, "Combustion of Boron Particles: Experiment and Theory," *Fourteenth Symposium (International) on Combustion,* The Combustion Institute, Pittsburgh, pp. 1401-1411 (1972).

4. S.C. Li and F. A. Williams, "Ignition and Combustion of Boron in Wet and Dry Atmospheres," *Twenty-Third Symposium (International) on Combustion*, The Combustion Institute, Pittsburgh, pp. 1147-1154 (1990).

5. S.C. Li and F. A. Williams, "Ignition and Combustion of Boron Particles," *Combustion of Boron-Based Propellants and Solid Fuels*, eds. K. K. Kuo and R. Pein, (Begell House Publishing Co. and CRC Press, 1993) pp. 248-271.

6. S. Yuasa and H. Isoda, "Ignition and Combustion of Small Boron Lumps in an Oxygen Stream," *Combustion and Flame* **86**, pp. 216-222 (1991).

7. H. Krier, R.L. Burton, M. J. Spalding, and T.J. Rood, "Ignition Dynamics of Boron Particles in a Shock Tube," *Journal of Propulsion and Power*, in press (1998). ; *ibid.*, AIAA 97-3234, Presented at the *33rd AIAA/ASME/SAE/ASEE Joint Propulsion Conference,* Seattle, WA, July 6-9 (1997).

8. R.O. Foelsche, R. L. Burton, and H. Krier, "High-pressure Ignition and Combustion of Boron Particles at 30-150 Atmospheres," *Combustion and Flame*, in press, CF97-085; *ibid.*, "High-pressure Ignition of Boron Particles in Oxygen/Water Vapor /Diluent Mixtures," AIAA Paper No 95-2120, presented at 30th AIAA Thermophysics Conference, San Diego, CA (June 1995).

9. I. Glassman, F.A. Williams, and P. Antaki, " A Physical and Chemical Interpretation of Boron Particle Combustion," *Twentieth Symposium (International) on Combustion*, The Combustion Institute, Pittsburgh, pp. 2057-2064 (1984).

10. M.K. King, "Boron Particle Ignition in Hot Gas Streams," *Combustion Science and Technology*, **8**, pp. 255-273 (1974).

11. M.K. King, "Single Particle Boron Ignition Modeling," *19th JANNAF Combustion Science and Technology*, Vol. II, CPIA Publication 366, pp. 27-42 (1982).

12. M.K. King, "Modifications of Boron Ignition Model to Include Recent Liquid Boron Oxide - Water Gas Kinetics," 26th JANNAF Combustion Meeting, Vol. II, CPIA Publication 529, pp. 203-207 (1989).

13. C. L. Yeh and K.K. Kuo, "Ignition and Combustion of Boron Particles," *Progress in Energy and Combustion Science,* **22**, 511-541 (1996).

14. R. A. Yetter, H. Rabitz, F. L Dryer, R.C. Brown, C.E. Kolb, "Kinetics of High-Temperature Chemistry," *Combustion and Flame* **83**, 43-62 (1991).

15. R. C. Brown, C.E. Kolb, R. A. Yetter, F. L Dryer, and H. Rabitz, " Kinetic Modeling and Sensitivity Analysis for B/H/O/C/F Combinations Systems," *Combustion and Flame* **101**, pp. 221-238 (1995).

16. L. Pasternack, "Gas-Phase Modeling of Homogeneous Boron/Oxygen/Hydrogen/Carbon Combustion," *Combustion and Flame* **90**, 259-268 (1992).

17. R.J. Kee, J. A. Miller, and T.H. Jefferson, "CHEMKIN: A General- Purpose, Problem-Independent, Transportable, *Fortran* Chemical Kinetics Code Package," SAND80-8003, Sandia National Laboratory, Livermore, CA (1980).

18. A.E. Lutz, R. J. Kee, and J. A. Miller, "SENKIN: A *Fortran* Program for Predicting Homogeneous Gas Phase Chemical Kinetics with Sensitivity Analysis," SAND87-8248, Sandia National Laboratory, Livermore, CA (1988).

19. W.T. Rawlins, R.R. Foutter, and T.E. Parker, Physical Sciences, Inc., "High Temperature Ignition of Coated Boron Particles in a Shock Tube," Workshop on Boron Combustion & Ingredient Chemistry, Penn State University, State College, PA (June 1995).

20. D.G. Keil, E.L. Dreizin, W. Felder, and H.F. Calcote, "Coating Effect on Boron Combustion," Workshop on Boron Combustion & Ingredient Chemistry, Penn State University, State College, PA (June 1995).

21. J. Cueilleron, J.C. Viala, F. Thevenot, C. Brodhag, J.M. Dussuau, and A. El Biach, "The Evaluation of Boron Purity by means of Electrical Measurements ," *Journal of the Less-Common Metals* **59**, 27-33 (1978).

22. P.C. Hiemenz and R. Rajagopalan, "Adsorption at Gas-Solid Interfaces," in *Principles of Colloid and Surface Chemistry*, (Marcel Dekker, Inc., NY, 1997) pp. 405-461.

23. K. K. Kuo, "Spray Statistics," in *Principles of Combustion*, (Wiley & Sons, NY, 1986) p. 523.

24. R. Naslain, "Boron Synthesis," in *Preparative Methods in Solid State Chemistry*, (Academic Press, NY, 1972) pp. 39-485.

25. J.K. Rice and T.P. Russell, unpublished results, NRL, 1995.

APPENDIX A:

The following are tables of the size distributions taken from the SEM photographs and several other calculations based on the diameter of the particles. The two rows at the bottom of the list are the statistics for the columns and contain the average value and the sum of each column, respectively. Column A is the particle diameter. Column B is the number of particles in a given area. Column C is the interval size for the particle diameter. Column D is the surface area (SA) for a particle of the corresponding diameter in Column A. Column E is the surface area of all particle, i.e., column D * column B. Column F is the mass of the particle with the diameter given in column A. Column G is the surface area per gram of material. Column H is the surface area per particle times the number of particles with a given diameter normalized by the particle size interval (column D* column B* column C). Column I is the normalized mass in grams obtained by multiplying the particle mass by the number of particles time the particle size interval (column F* column B* column C). The sum of column J is the numerator of the square of the surface area diameter, D_{20} , corresponding to the particle diameter in column A. This is defined in equation 2:

$$(D_{20})^{2-0} = \int D^2 F(D)\, dD / \int D^0 F(D)\, dD \qquad (3)$$

where F(D) is the particle size distribution function and D is the particle diameter and the integrals are taken from zero to infinity. Column J is obtained by taking column A^2 * column B * column C. The sum of the denominator of this equation is given in column L and is obtained by taking column B* column C. A more general equation is obtained by substituting j for 2 and k for 0. The sum of column K is the numerator of the Sauter diameter equation given in equation 3. See reference 23 for further discussion.

$$(D_{32})^{3-2} = \int D^3 F(D)\, dD / \int D^2 F(D)\, dD \qquad (4)$$

Column K is obtained by taking column A^3 * column B * column C. The denominator of this equation is the same as the sum of column J, i.e., the numerator of the D_{20} value.

Sample 3

	A	B	C	D	E	F	G	H	I	J	K	L
1	diameter	# part.	intervals	SA (m2/p)	SA all part.	Part. Mass	SA/m (m2/g)	norm. SA	norm g	num D20	num D32	part*interv
2	0.08	15	0.08	2.04E-14	1.21	6.44E-16	31.71	2.47E-14	7.78E-16	0.01	0.00	1.21
3	0.16	100	0.08	8.16E-14	8.06	5.15E-15	15.86	6.58E-13	4.15E-14	0.21	0.03	8.06
4	0.24	105	0.08	1.84E-13	8.46	1.74E-14	10.57	1.55E-12	1.47E-13	0.49	0.12	8.46
5	0.32	85	0.08	3.27E-13	6.85	4.12E-14	7.93	2.24E-12	2.82E-13	0.71	0.23	6.85
6	0.40	50	0.08	5.10E-13	4.03	8.04E-14	6.34	2.06E-12	3.24E-13	0.65	0.26	4.03
7	0.48	65	0.08	7.35E-13	5.24	1.39E-13	5.29	3.85E-12	7.28E-13	1.23	0.59	5.24
8	0.56	25	0.08	1.00E-12	2.02	2.21E-13	4.53	2.02E-12	4.45E-13	0.64	0.36	2.02
9	0.64	25	0.08	1.31E-12	2.02	3.29E-13	3.96	2.63E-12	6.64E-13	0.84	0.54	2.02
10	0.73	5	0.08	1.65E-12	0.40	4.69E-13	3.52	6.66E-13	1.89E-13	0.21	0.15	0.40
11	0.81	10	0.08	2.04E-12	0.81	6.44E-13	3.17	1.64E-12	5.19E-13	0.52	0.42	0.81
12	0.89	5	0.08	2.47E-12	0.40	8.57E-13	2.88	9.95E-13	3.45E-13	0.32	0.28	0.40
13	0.97	10	0.08	2.94E-12	0.81	1.11E-12	2.64	2.37E-12	8.96E-13	0.75	0.73	0.81
14	1.05	0	0.08	3.45E-12	0.00	1.41E-12	2.44	0.00E+00	0.00E+00	0.00	0.00	0.00
15	1.13	5	0.08	4.00E-12	0.40	1.77E-12	2.27	1.61E-12	7.12E-13	0.51	0.58	0.40
16	1.21	3	0.08	4.59E-12	0.24	2.17E-12	2.11	1.11E-12	5.25E-13	0.35	0.43	0.24
17	1.29	0	0.08	5.22E-12	0.00	2.64E-12	1.98	0.00E+00	0.00E+00	0.00	0.00	0.00
18	1.37	0	0.08	5.90E-12	0.00	3.16E-12	1.87	0.00E+00	0.00E+00	0.00	0.00	0.00
19	1.45	0	0.08	6.61E-12	0.00	3.75E-12	1.76	0.00E+00	0.00E+00	0.00	0.00	0.00
20	1.53	0	0.08	7.37E-12	0.00	4.41E-12	1.67	0.00E+00	0.00E+00	0.00	0.00	0.00
21	1.61	0	0.08	8.16E-12	0.00	5.15E-12	1.59	0.00E+00	0.00E+00	0.00	0.00	0.00
22	1.69	1	0.08	9.00E-12	0.08	5.96E-12	1.51	7.25E-13	4.80E-13	0.23	0.39	0.08
23	1.77	0	0.08	9.88E-12	0.00	6.85E-12	1.44	0.00E+00	0.00E+00	0.00	0.00	0.00
24	1.85	0	0.08	1.08E-11	0.00	7.83E-12	1.38	0.00E+00	0.00E+00	0.00	0.00	0.00
25	1.93	0	0.08	1.18E-11	0.00	8.90E-12	1.32	0.00E+00	0.00E+00	0.00	0.00	0.00
26	2.02	0	0.08	1.28E-11	0.00	1.01E-11	1.27	0.00E+00	0.00E+00	0.00	0.00	0.00
27	2.10	0	0.08	1.38E-11	0.00	1.13E-11	1.22	0.00E+00	0.00E+00	0.00	0.00	0.00
28	2.18	0	0.08	1.49E-11	0.00	1.27E-11	1.17	0.00E+00	0.00E+00	0.00	0.00	0.00
29	2.26	0	0.08	1.60E-11	0.00	1.41E-11	1.13	0.00E+00	0.00E+00	0.00	0.00	0.00
30	2.34	0	0.08	1.72E-11	0.00	1.57E-11	1.09	0.00E+00	0.00E+00	0.00	0.00	0.00
31	2.42	0	0.08	1.84E-11	0.00	1.74E-11	1.06	0.00E+00	0.00E+00	0.00	0.00	0.00
32	2.50	0	0.08	1.96E-11	0.00	1.92E-11	1.02	0.00E+00	0.00E+00	0.00	0.00	0.00
33	2.58	0	0.08	2.09E-11	0.00	2.11E-11	0.99	0.00E+00	0.00E+00	0.00	0.00	0.00
34	2.66	1	0.08	2.22E-11	0.08	2.31E-11	0.96	1.79E-12	1.86E-12	0.57	1.52	0.08
35	2.74	0	0.08	2.36E-11	0.00	2.53E-11	0.93	0.00E+00	0.00E+00	0.00	0.00	0.00
36												
37	1.41	15	0.08	8.21E-12	1.21	6.70E-12	3.84	7.63E-13	2.40E-13	0.24	0.20	1.21
38												
39	47.96	510	2.74	2.79E-10	41.11	2.28E-10	130.60	2.59E-11	8.16E-12	8.26	6.64	41.11

Sample 4

	A	B	C	D	E	F	G	H	I	J	K	L
1	diameter	# particles	intervals	SA (m2/p)	SA all part.	Part. Mass	SA/m (m2/g)	norm. SA	norm g	num D20	num D32	part.*interv
2	0.07	75	0.08	1.54E-14	6.00	4.22E-16	36.51	9.24E-14	2.53E-15	0.03	0.00	6.00
3	0.13	50	0.08	5.31E-14	4.00	2.70E-15	19.66	2.12E-13	1.08E-14	0.07	0.01	4.00
4	0.20	25	0.08	1.26E-13	2.00	9.83E-15	12.78	2.51E-13	1.97E-14	0.08	0.02	2.00
5	0.27	25	0.08	2.29E-13	2.00	2.42E-14	9.47	4.58E-13	4.84E-14	0.15	0.04	2.00
6	0.30	40	0.08	2.83E-13	3.20	3.32E-14	8.52	9.05E-13	1.06E-13	0.29	0.09	3.20
7	0.50	100	0.08	7.85E-13	8.00	1.54E-13	5.11	6.28E-12	1.23E-12	2.00	1.00	8.00
8	0.60	25	0.08	1.13E-12	2.00	2.65E-13	4.26	2.26E-12	5.31E-13	0.72	0.43	2.00
9	0.70	36	0.08	1.54E-12	2.88	4.22E-13	3.65	4.43E-12	1.21E-12	1.41	0.99	2.88
10	0.80	50	0.08	2.01E-12	4.00	6.29E-13	3.20	8.04E-12	2.52E-12	2.56	2.05	4.00
11	0.90	25	0.08	2.54E-12	2.00	8.96E-13	2.84	5.09E-12	1.79E-12	1.62	1.46	2.00
12	1.00	24	0.08	3.14E-12	1.92	1.23E-12	2.56	6.03E-12	2.36E-12	1.92	1.92	1.92
13	1.20	50	0.08	4.52E-12	4.00	2.12E-12	2.13	1.81E-11	8.50E-12	5.76	6.91	4.00
14	1.30	64	0.08	5.31E-12	5.12	2.70E-12	1.97	2.72E-11	1.38E-11	8.65	11.25	5.12
15	1.70	5	0.08	9.08E-12	0.40	6.04E-12	1.50	3.63E-12	2.42E-12	1.16	1.97	0.40
16	2.00	15	0.08	1.26E-11	1.20	9.83E-12	1.28	1.51E-11	1.18E-11	4.80	9.60	1.20
17	2.30	3	0.08	1.66E-11	0.24	1.50E-11	1.11	3.99E-12	3.59E-12	1.27	2.92	0.24
18	2.60	3	0.08	2.12E-11	0.24	2.16E-11	0.98	5.10E-12	5.18E-12	1.62	4.22	0.24
19	3.00	13	0.08	2.83E-11	1.04	3.32E-11	0.85	2.94E-11	3.45E-11	9.36	28.08	1.04
20	3.30	1	0.08	3.42E-11	0.08	4.42E-11	0.77	2.74E-12	3.53E-12	0.87	2.87	0.08
21	3.70	3	0.08	4.30E-11	0.24	6.23E-11	0.69	1.03E-11	1.49E-11	3.29	12.16	0.24
22	4.00	1	0.08	5.03E-11	0.08	7.87E-11	0.64	4.02E-12	6.29E-12	1.28	5.12	0.08
23	4.30	0	0.08	5.81E-11	0.00	9.77E-11	0.59	0.00E+00	0.00E+00	0.00	0.00	0.00
24	4.70	0	0.08	6.94E-11	0.00	1.28E-10	0.54	0.00E+00	0.00E+00	0.00	0.00	0.00
25	5.00	0	0.08	7.85E-11	0.00	1.54E-10	0.51	0.00E+00	0.00E+00	0.00	0.00	0.00
26	5.30	1	0.08	8.82E-11	0.08	1.83E-10	0.48	7.06E-12	1.46E-11	2.25	11.91	0.08
27	5.70	0	0.08	1.02E-10	0.00	2.28E-10	0.45	0.00E+00	0.00E+00	0.00	0.00	0.00
28	6.00	1	0.08	1.13E-10	0.08	2.65E-10	0.43	9.05E-12	2.12E-11	2.88	17.28	0.08
29	6.30	0	0.08	1.25E-10	0.00	3.07E-10	0.41	0.00E+00	0.00E+00	0.00	0.00	0.00
30	6.70	1	0.08	1.41E-10	0.08	3.70E-10	0.38	1.13E-11	2.96E-11	3.59	24.06	0.08
31	7.00	0	0.08	1.54E-10	0.00	4.22E-10	0.37	0.00E+00	0.00E+00	0.00	0.00	0.00
32	7.30	0	0.08	1.67E-10	0.00	4.78E-10	0.35	0.00E+00	0.00E+00	0.00	0.00	0.00
33	7.70	1	0.08	1.86E-10	0.08	5.61E-10	0.33	1.49E-11	4.49E-11	4.74	36.52	0.08
34	8.00	0	0.08	2.01E-10	0.00	6.29E-10	0.32	0.00E+00	0.00E+00	0.00	0.00	0.00
35												
36	3.17	19	0.08	5.21E-11	1.54	1.24E-10	3.81	5.94E-12	6.81E-12	1.89	5.54	1.54
37												
38	104.57	637	2.64	1.72E-09	50.96	4.10E-09	125.65	1.96E-10	2.25E-10	62.36	182.87	50.96

Sample 5

	A	B	C	D	E	F	G	H	I	J	K	L
1	diameter	# particles	intervals	SA (m2/p)	SA all part.	Part. Mass	SA/m (m2/g)	norm. SA	norm g	num D20	norm D32	part.*interv
2	0.08	33	0.08	2.04E-14	2.66	6.44E-16	31.71	5.43E-14	1.71E-15	0.02	0.00	2.66
3	0.16	24	0.16	8.16E-14	3.87	5.15E-15	15.86	3.16E-13	1.99E-14	0.10	0.02	3.87
4	0.32	25	0.16	3.27E-13	4.03	4.12E-14	7.93	1.32E-12	1.66E-13	0.42	0.14	4.03
5	0.48	13	0.16	7.35E-13	2.10	1.39E-13	5.29	1.54E-12	2.91E-13	0.49	0.24	2.10
6	0.64	11	0.16	1.31E-12	1.77	3.29E-13	3.96	2.32E-12	5.84E-13	0.74	0.48	1.77
7	0.81	6	0.16	2.04E-12	0.97	6.44E-13	3.17	1.97E-12	6.22E-13	0.63	0.51	0.97
8	0.97	11	0.16	2.94E-12	1.77	1.11E-12	2.64	5.21E-12	1.97E-12	1.66	1.60	1.77
9	1.13	2	0.16	4.00E-12	0.32	1.77E-12	2.27	1.29E-12	5.69E-13	0.41	0.46	0.32
10	1.29	2	0.16	5.22E-12	0.32	2.64E-12	1.98	1.68E-12	8.50E-13	0.54	0.69	0.32
11	1.45	5	0.16	6.61E-12	0.81	3.75E-12	1.76	5.33E-12	3.03E-12	1.70	2.46	0.81
12	1.61	5	0.16	8.16E-12	0.81	5.15E-12	1.59	6.58E-12	4.15E-12	2.09	3.38	0.81
13	1.77	3	0.16	9.88E-12	0.48	6.85E-12	1.44	4.78E-12	3.31E-12	1.52	2.70	0.48
14	1.93	3	0.16	1.18E-11	0.48	8.90E-12	1.32	5.68E-12	4.30E-12	1.81	3.50	0.48
15	2.10	2	0.16	1.38E-11	0.32	1.13E-11	1.22	4.45E-12	3.65E-12	1.42	2.97	0.32
16	2.26	3	0.16	1.60E-11	0.48	1.41E-11	1.13	7.74E-12	6.83E-12	2.46	5.56	0.48
17	2.42	2	0.16	1.84E-11	0.32	1.74E-11	1.06	5.92E-12	5.60E-12	1.88	4.56	0.32
18	2.58	2	0.16	2.09E-11	0.32	2.11E-11	0.99	6.74E-12	6.80E-12	2.14	5.53	0.32
19	2.74	2	0.16	2.36E-11	0.32	2.53E-11	0.93	7.61E-12	8.15E-12	2.42	6.63	0.32
20	2.90	0	0.16	2.64E-11	0.00	3.00E-11	0.88	0.00E+00	0.00E+00	0.00	0.00	0.00
21	3.06	2	0.16	2.95E-11	0.32	3.53E-11	0.83	9.50E-12	1.14E-11	3.02	9.26	0.32
22	3.22	2	0.16	3.27E-11	0.32	4.12E-11	0.79	1.05E-11	1.33E-11	3.35	10.80	0.32
23	3.39	1	0.16	3.60E-11	0.16	4.77E-11	0.76	5.80E-12	7.69E-12	1.85	6.25	0.16
24	3.55	1	0.16	3.95E-11	0.16	5.48E-11	0.72	6.37E-12	8.84E-12	2.03	7.19	0.16
25	3.71	0	0.16	4.32E-11	0.00	6.26E-11	0.69	0.00E+00	0.00E+00	0.00	0.00	0.00
26	3.87	2	0.16	4.70E-11	0.32	7.12E-11	0.66	1.52E-11	2.29E-11	4.83	18.67	0.32
27	4.03	0	0.16	5.10E-11	0.00	8.04E-11	0.63	0.00E+00	0.00E+00	0.00	0.00	0.00
28	4.19	0	0.16	5.52E-11	0.00	9.05E-11	0.61	0.00E+00	0.00E+00	0.00	0.00	0.00
29	4.35	0	0.16	5.95E-11	0.00	1.01E-10	0.59	0.00E+00	0.00E+00	0.00	0.00	0.00
30	4.51	0	0.16	6.40E-11	0.00	1.13E-10	0.57	0.00E+00	0.00E+00	0.00	0.00	0.00
31	4.67	0	0.16	6.87E-11	0.00	1.26E-10	0.55	0.00E+00	0.00E+00	0.00	0.00	0.00
32	4.84	0	0.16	7.35E-11	0.00	1.39E-10	0.53	0.00E+00	0.00E+00	0.00	0.00	0.00
33	5.00	0	0.16	7.84E-11	0.00	1.53E-10	0.51	0.00E+00	0.00E+00	0.00	0.00	0.00
34	5.16	0	0.16	8.36E-11	0.00	1.69E-10	0.50	0.00E+00	0.00E+00	0.00	0.00	0.00

Sample 5

	A	B	C	D	E	F	G	H	I	J	K	L
35	5.32	0	0.16	8.89E-11	0.00	1.85E-10	0.48	0.00E+00	0.00E+00	0.00	0.00	0.00
36	5.48	2	0.16	9.44E-11	0.32	2.02E-10	0.47	3.04E-11	6.52E-11	9.68	53.08	0.32
37	5.64	0	0.16	1.00E-10	0.00	2.21E-10	0.45	0.00E+00	0.00E+00	0.00	0.00	0.00
38	5.80	1	0.16	1.06E-10	0.16	2.40E-10	0.44	1.71E-11	3.87E-11	5.43	31.50	0.16
39	5.96	0	0.16	1.12E-10	0.00	2.61E-10	0.43	0.00E+00	0.00E+00	0.00	0.00	0.00
40	6.13	0	0.16	1.18E-10	0.00	2.82E-10	0.42	0.00E+00	0.00E+00	0.00	0.00	0.00
41	6.29	0	0.16	1.24E-10	0.00	3.05E-10	0.41	0.00E+00	0.00E+00	0.00	0.00	0.00
42	6.45	0	0.16	1.31E-10	0.00	3.29E-10	0.40	0.00E+00	0.00E+00	0.00	0.00	0.00
43	6.61	0	0.16	1.37E-10	0.00	3.55E-10	0.39	0.00E+00	0.00E+00	0.00	0.00	0.00
44	6.77	0	0.16	1.44E-10	0.00	3.81E-10	0.38	0.00E+00	0.00E+00	0.00	0.00	0.00
45	6.93	0	0.16	1.51E-10	0.00	4.09E-10	0.37	0.00E+00	0.00E+00	0.00	0.00	0.00
46	7.09	1	0.16	1.58E-10	0.16	4.39E-10	0.36	2.55E-11	7.07E-11	8.11	57.52	0.16
47	7.25	0	0.16	1.65E-10	0.00	4.69E-10	0.35	0.00E+00	0.00E+00	0.00	0.00	0.00
48												
49	3.63	4	0.16	5.57E-11	0.52	1.20E-10	2.20	4.15E-12	6.30E-12	1.32	5.12	0.52
50												
51	166.92	170	7.49	2.62E-09	24.62	5.63E-09	103.61	1.95E-10	2.96E-10	62.07	235.70	24.10

Sample 6

	A	B	C	D	E	F	G	H	I	J	K	L
1	diameter	# particles	intervals	SA (m2/p)	SA all part.	Part. Mass	SA/m (m2/g)	norm. SA	norm g	num D20	num D32	part.* interv
2	0.09	1,100	0.55	2.27E-14	605	7.55E-16	30.07	1.37E-11	4.57E-13	4	0	605
3	0.85	662	0.75	2.27E-12	497	7.55E-13	3.01	1.13E-09	3.75E-10	359	305	497
4	1.60	132	0.90	8.04E-12	119	5.03E-12	1.60	9.55E-10	5.98E-10	304	487	119
5	2.50	30	2.50	1.96E-11	75	1.92E-11	1.02	1.47E-09	1.44E-09	469	1172	75
6	5.00	24	2.50	7.85E-11	60	1.54E-10	0.51	4.71E-09	9.22E-09	1500	7500	60
7	7.50	10	2.50	1.77E-10	25	5.19E-10	0.34	4.42E-09	1.30E-08	1406	10547	25
8	10.00	5	2.50	3.14E-10	13	1.23E-09	0.26	3.93E-09	1.54E-08	1250	12500	13
9	12.50	2	2.50	4.91E-10	4	2.40E-09	0.20	1.84E-09	9.00E-09	586	7324	4
10	15.00	1	2.50	7.07E-10	1	4.15E-09	0.17	8.84E-10	5.19E-09	281	4219	1
11	17.50	1	2.50	9.62E-10	1	6.59E-09	0.15	1.20E-09	8.23E-09	383	6699	1
12	20.00	0	2.50	1.26E-09	0	9.83E-09	0.13	0.00E+00	0.00E+00	0	0	0
13	22.50	0	2.50	1.59E-09	0	1.40E-08	0.11	0.00E+00	0.00E+00	0	0	0
14	25.00	1	2.50	1.96E-09	1	1.92E-08	0.10	2.45E-09	2.40E-08	781	19531	1
15	27.50	0	2.50	2.38E-09	0	2.56E-08	0.09	0.00E+00	0.00E+00	0	0	0
16	30.00	0	2.50	2.83E-09	0	3.32E-08	0.09	0.00E+00	0.00E+00	0	0	0
17	32.50	0	2.50	3.32E-09	0	4.22E-08	0.08	0.00E+00	0.00E+00	0	0	0
18	35.00	0	2.50	3.85E-09	0	5.27E-08	0.07	0.00E+00	0.00E+00	0	0	0
19	37.50	0	2.50	4.42E-09	0	6.48E-08	0.07	0.00E+00	0.00E+00	0	0	0
20												
21	16.81	109	2.21	1.35E-09	78	1.54E-08	2.11	1.28E-09	4.80E-09	407	3905	78
22												
23	302.54	2,075	41.91	2.57E-08	1478	2.92E-07	40.18	2.43E-08	9.12E-08	7730	70284	1400

Sample 7

	A	B	C	D	E	F	G	H	I	J	K	L
1	diameter	# particles	intervals	SA (m2/p)	SA all part.	Part. Mass	SA/m (m2/g)	norm. SA	norm g	num D20	num D32	part.*interv
2	0.08	22,950	0.08	2.04E-14	1850	6.44E-16	31.71	3.78E-11	1.19E-12	12	1	1850
3	0.16	6,520	0.16	8.16E-14	1051	5.15E-15	15.86	8.58E-11	5.41E-12	27	4	1051
4	0.32	4,950	0.16	3.27E-13	798	4.12E-14	7.93	2.61E-10	3.29E-11	83	27	798
5	0.48	1,120	0.32	7.24E-13	361	1.36E-13	5.33	2.61E-10	4.91E-11	83	40	361
6	0.81	225	0.16	2.04E-12	36	6.44E-13	3.17	7.40E-11	2.33E-11	24	19	36
7	0.97	125	0.16	2.94E-12	20	1.11E-12	2.64	5.92E-11	2.24E-11	19	18	20
8	1.12	60	1.30	3.94E-12	78	1.73E-12	2.28	3.07E-10	1.35E-10	98	110	78
9	2.50	6	2.50	1.96E-11	15	1.92E-11	1.02	2.95E-10	2.88E-10	94	234	15
10	5.00	28	2.50	7.85E-11	70	1.54E-10	0.51	5.50E-09	1.08E-08	1750	8750	70
11	7.50	2	5.00	1.77E-10	10	5.19E-10	0.34	1.77E-09	5.19E-09	563	4219	10
12	12.50	3	2.50	4.91E-10	8	2.40E-09	0.20	3.68E-09	1.80E-08	1172	14648	8
13	15.00	3	2.50	7.07E-10	8	4.15E-09	0.17	5.30E-09	3.11E-08	1688	25313	8
14	17.50	2	2.50	9.62E-10	5	6.59E-09	0.15	4.81E-09	3.29E-08	1531	26797	5
15	20.00	4	2.50	1.26E-09	10	9.83E-09	0.13	1.26E-08	9.83E-08	4000	80000	10
16	25.00	15	5.00	1.96E-09	75	1.92E-08	0.10	1.47E-07	1.44E-06	46875	1171875	75
17	30.00	4	5.00	2.83E-09	20	3.32E-08	0.09	5.65E-08	6.64E-07	18000	540000	20
18	32.00	4	2.50	3.22E-09	10	4.03E-08	0.08	3.22E-08	4.03E-07	10240	327680	10
19	35.00	3	2.50	3.85E-09	8	5.27E-08	0.07	2.89E-08	3.95E-07	9188	321563	8
20	37.50	3	2.50	4.42E-09	8	6.48E-08	0.07	3.31E-08	4.86E-07	10547	395508	8
21	42.50	2	5.00	5.67E-09	10	9.43E-08	0.06	5.67E-08	9.43E-07	18063	767656	10
22	45.00	1	2.50	6.36E-09	3	1.12E-07	0.06	1.59E-08	2.80E-07	5063	227813	3
23	50.00	1	5.00	7.85E-09	5	1.54E-07	0.05	3.93E-08	7.68E-07	12500	625000	5
24												
25	17.32	1,638	2.38	1.81E-09	203	2.70E-08	3.27	2.02E-08	2.53E-07	6437	206240	203
26												
27	380.94	36,031	52.35	3.99E-08	4457	5.94E-07	72.02	4.45E-07	5.58E-06	141617	4537274	4457